Available online at www.sciencedirect.com
ScienceDirect
Polymer 48 (2007) 1641–1650
polymer
www.elsevier.com/locate/polymer

The phase structures of nylon 6.6 as studied by temperature-modulated calorimetry and their link to X-ray structure and molecular motion☆

Wulin Qiu [a], Anton Habenschuss [b], Bernhard Wunderlich [a,b,*]

[a] Department of Chemistry, The University of Tennessee, Knoxville, TN 37996-1600, USA
[b] Chemical Sciences Division, Oak Ridge National Laboratory, Oak Ridge, TN 37831-6197, USA

Received 6 December 2006; received in revised form 14 January 2007; accepted 15 January 2007
Available online 19 January 2007

Abstract

The phase behavior of semicrystalline, dry nylon 6.6 is analyzed on the basis of differential scanning calorimetry, DSC, and quasi-isothermal, temperature-modulated DSC, TMDSC. The data were collected over the temperature range from below the glass transitions to above the isotropization. Based on the contributions of the vibrational motion to the heat capacity, as is available from the ATHAS Data Bank, and the multifaceted new calorimetry, as well as on information on X-ray diffraction, molecular dynamics simulation of paraffin crystals, and quasi-elastic neutron scattering, the following observations are made: (a) beginning at the glass transition temperature of the mobile-amorphous phase ($T_g = 323$ K), a broadened transition of the semicrystalline sample is observed which reaches to 342 K ($T_g = 332.7$ K). An additional rigid-amorphous phase, RAF, undergoes its separate, broad glass transition immediately thereafter (340–400 K, $T_g \approx 370$ K). (b) The transition of the RAF, in turn, overlaps with increasing large-amplitude motion of the CH_2 groups within the crystals and latent heat effects due to melting, recrystallization, and crystal annealing. (c) From 390 to 480 K the heat capacity of the crystals increasingly exceeds that of the melt due to additional entropy (disordering) contributions. Above 440 K, close to the Brill temperature, the heat capacity seems to drop to the level of the melt. (d) If observation (c) is confirmed, some locally reversible melting is present on the crystal surfaces. (e) The increasing large-amplitude motion is described as a glass transition of the crystals, occurring below the melting point, at 409 K. The assumption of a separate glass transition in the ordered phase was previously successful in analyzing aliphatic poly(oxide)s and mesophases. The full description of the globally metastable, semicrystalline phase structure of nylons, thus, needs information on the glass transitions of the two amorphous phases *and* the ordered phase and the various irreversible and locally reversible order/order transitions and their kinetics.
Published by Elsevier Ltd.

Keywords: Polymer science; Nylon 6.6; Melting

1. Introduction

The aliphatic polyamides, as developed by Carothers [1], were the basis of the first commercially successful semicrystalline, synthetic fibers. Polyamide fibers are used for textiles and carpets and also, in bulk, as an engineering plastic [2]. The first fibers were introduced commercially in 1938 under the trade name ''Nylon'' (DuPont de Nemours and Co.) which by now is the generic term for these polyamides. The basic chemical structure consists of methylene sequences, interrupted at regular intervals by intermolecularly hydrogen-bonded amide groups. The specific polymer of this research, nylon 6.6, is represented by the repeating unit [NH–CO–$(CH_2)_4$–CO–NH–$(CH_2)_6$–]. The dimensions of the essentially planar amide group in nylon were established in 1953, based on the structure of crystalline peptides [3]. The capability of nylon to form hydrogen bonds is also retained in the melt. The methylene units in the crystal try to assume a planar zig-zag chain consisting of *trans*-conformations, established

☆ ''The submitted manuscript has been authored by a contractor of the U.S. Government under the contract no. DOE-AC05-00OR22725. Accordingly, the U.S. Government retains a non-exclusive, royalty-free license to publish, or reproduce the published form of this contribution, or allow others to do so, for U.S. Government purposes.''

* Corresponding author. Department of Chemistry, The University of Tennessee, Knoxville, TN 37996-1600, USA. Tel./fax: +1 865 675 4532.
E-mail address: wunderlich@chartertn.net (B. Wunderlich).

0032-3861/$ - see front matter Published by Elsevier Ltd.
doi:10.1016/j.polymer.2007.01.024

at low temperatures as the low-energy shape in paraffins and polyethylene [4].

The crystal structures of the aliphatic nylons have been summarized, for example, in Ref. [5]. Specifically, the chains of nylon 6.6 are non-polar (symmetric along the chain directions), and in the most common, triclinic α-crystals they are connected by hydrogen bonds to sheets in the crystallographic *ac*-planes which are stacked at an angle of $\alpha = 48.5°$ [6–8]. At low temperature, the heat capacity, C_p, of the nylon crystals is fully described by vibrational contributions [9] which reproduce the experimental data, critically evaluated in the ATHAS Data Bank [10]. The amorphous nylon 6.6 can be described from about 50 K to the glass transition temperature, T_g (=323 K), by the same vibrational C_p [11]. The equilibrium melting temperature, T_m^o, for nylon 6.6 is taken to be 574 K and the heat of fusion of a fully crystalline sample to be 57.8 kJ mol^{-1} (or 255.4 J g^{-1}) based on the extensive discussions of a wide range of literature data [12–14].

A broad transition of the crystal structure, named after Brill [15], is reported in nylon 6.6 between 450 and 490 K and is accompanied by changes in the thermal and mechanical properties [2]. Crystallographically, this transition is observed as a gradual transformation from the diffraction patterns with triclinic to pseudo-hexagonal symmetry, accompanied by a 12% increase in unit cell volume [16]. The increase in crystal symmetry at the Brill transition causes a marked increase in segmental mobility of the methylene groups, as was seen already in early NMR studies [17]. The segmental motion was then studied by solid-state deuterium NMR and molecular dynamics simulations using selectively deuterated samples [18–20]. It was found that in the crystal the N–D- and C–D-group undergoes spatially heterogeneous librations, both below and above the Brill transition. At 500 K, the amplitude of the motion in the crystals becomes very large, reaching an angle of 60° for all methylene groups. The hydrogen bonds, however, are found to remain largely intact. In the amorphous part, limited librations and internal rotations start below T_g, while above T_g both N–D- and C–D-site perform nearly isotropic motion. Quasi-elastic neutron scattering studies on samples of nylon 6.6 with different crystallinities, similarly, showed that at temperatures 40 K below melting, the CH_2 groups in the crystal undergo already large-amplitude, liquid-like motion [21].

The effect of this large-amplitude motion of the CH_2 groups below the melting temperature of the crystals of nylon 6.6 was also linked to the excess in C_p, using extensive comparisons of samples of different thermal history, analyzed by standard differential scanning calorimetry (DSC) and X-ray diffraction [22]. In this paper the contribution of the large-amplitude motion to C_p is separated quantitatively from the latent heat effects due to crystal perfection, recrystallization, and locally reversible melting using temperature-modulated DSC (TMDSC) [23]. The results are linked to similar large-amplitude motion effects first seen for polyethylene [24] and detailed in Ref. [25], and the glass transitions of crystals of aliphatic poly(oxide)s [26] and mesophases [27,28].

2. Experimental

2.1. Materials

The nylon 6.6 [structure-based name: poly(iminoadipoyliminohexamethylene), source-based name: poly(hexamethylene adipamide)] used in this research has an estimated viscosity-average molar mass, M_v, of 15–20 kDa and was purchased from Scientific Polymer Products Inc. It was delivered in the form of translucent pellets with a density of about $d = 1.30$ mg m^{-3} (Lot 20, Cat. 033). At the glass transition temperature, the heat capacity, C_p, of the amorphous, glassy polymer increases by 115.5 J K^{-1} mol^{-1} [10]. Before measurement, the samples were melted by heating to 568 K to produce a dry sample, accompanied by the usual increase in molar mass [23]. Fig. 1a shows a characterization of the studied samples by standard DSC. After melting, the cooling curve at 10 K min^{-1} is the top DSC trace. This is followed by a second heating at 10 K min^{-1}. The weight loss due to water in such experiments was 3.4–4.5%. The DSC on heating after slow cooling by quasi-isothermal TMDSC (as shown in Fig. 2a, points ●, discussed below) is illustrated in the third curve of Fig. 1a. Estimates of the crystallinity were obtained from approximate baselines and the above mentioned heat of fusion. The standard DSC results follow closely the earlier, more extensive, DSC traces on nylon 6.6 (which also included data for several other nylons) [11].

2.2. Differential scanning calorimetry

The calorimetry was carried out with a Thermal Analyst 2920 system from TA Instruments, Inc. The twin calorimeter is of the isoperibol heat-flux type, capable of standard DSC and quasi-isothermal temperature-modulated DSC. The temperature measurement and modulation control are done by the sample-temperature sensor. During the experiments, a refrigerated cooling system with a cooling capability to about 220 K, was used, and dry N_2 gas with a flow rate of 25 mL min^{-1} was purged through the DSC cell. The temperature was calibrated in the standard DSC mode using the onset temperature of the melting-transition peak for indium at 429.75 K, and the heat-flow rate was pre-calibrated at a scanning rate of 10 K min^{-1} with the specific heat of fusion of indium of 28.62 J g^{-1} [29]. The melting temperature of indium was also measured in the quasi-isothermal TMDSC mode with a 0.5 K amplitude and 100 s period after calibration in the standard DSC mode, to identify any differences. It was found that quasi-isothermal TMDSC experiments after initial standard DSC calibration led to a melting temperature of 428.89 K. To correct the temperatures from the quasi-isothermal measurements, a constant of 0.86 K was added to the average temperatures of the quasi-isothermal measurements carried out at T_o.

In all the experiments, standard aluminum pans of 20 μL with covers were used for the sample and the empty as reference. A somewhat lighter reference pan was used for all measurements to approximately correct for the asymmetry of the

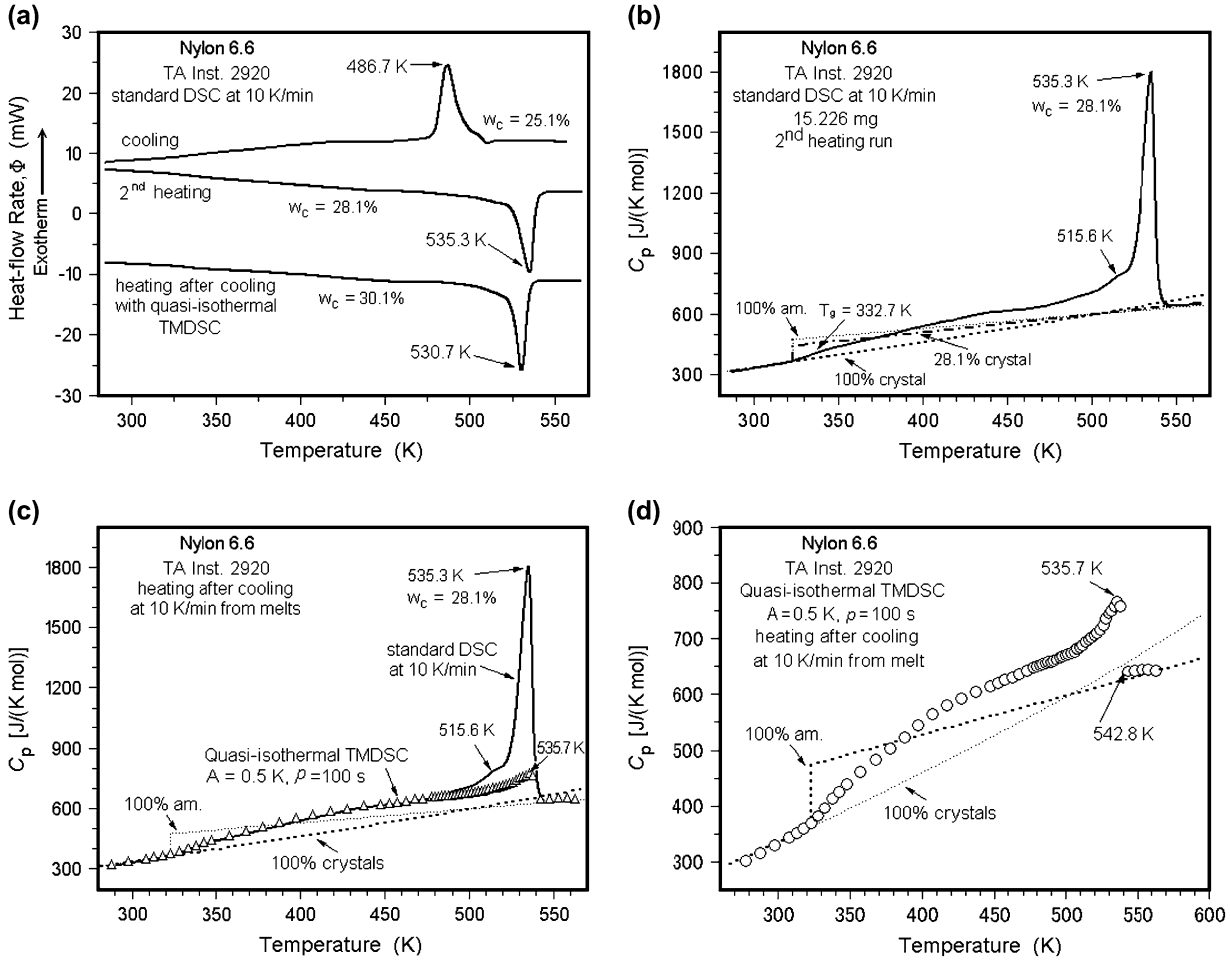

Fig. 1. Standard DSC at 10 K min^{-1} and TMDSC of nylon 6.6. (a) On cooling after an isotherm of 10 min at 568 K, followed by a second heating after a 10 min isotherm at 275 K (15.226 mg sample, top and center curves). Bottom curve, sample of 12.323 mg on heating after completion of quasi-isothermal cooling. (b) Analysis of the center curve of (a) by comparison with the ATHAS Data Bank information [10]. (c) Comparison of the center curve of (a) with a quasi-isothermal DSC run on a sample of 12.496 mg, cooled before at 10 K min^{-1} (as for the top curve). (d) Enlarged plot of the quasi-isothermal data of (c).

calorimeter [30]. The standard DSC on cooling and heating was performed at 10 K min^{-1}. All samples were cooled first from the melt at 560 K to about 280 K to produce the standard, dry nylon used in all further analysis. Isotherms of 10 min preceded and concluded the DSC experiments.

The quasi-isothermal TMDSC was carried out using sinusoidal modulation about successive base temperatures, T_o, with a modulation period of $p = 100$ s and a modulation amplitude of 0.5 K. The quasi-isothermal runs were used to calculate the apparent, reversing C_p ($= mc_p$):

$$mc_p = \frac{A_\Phi}{A_{T_s}\omega} \times \sqrt{1+\tau^2\omega^2}, \tag{1}$$

where m is the sample mass; c_p is the specific heat capacity in J K^{-1} g^{-1}; A_Φ is the amplitude of the modulated heat-flow rate and A_{T_s} is the amplitude of the temperature modulation with frequency ω ($= 2\pi/p$, where p is the period in s); and τ represents the calibration factor at the given conditions [31]. Note that the term "reversing" for C_p and other quantities is used when true reversibility has not been established. To measure the crystallinity of the sample, a standard DSC trace at 10 K min^{-1} was occasionally run immediately after the completion of the quasi-isothermal TMDSC, as shown in the bottom trace of Fig. 1a. Unless otherwise stated, the crystallinity, w_c, shown in the figures was calculated using an appropriately chosen baseline using the relationship:

$$w_c = \left(\Delta H(\text{measured})/\Delta H_f\right), \tag{2}$$

where ΔH_f is the (temperature-dependent) heat of fusion of fully crystalline nylon over the given temperature range.

3. Results and preliminary discussion of the data

3.1. Differential scanning calorimetry

The basic thermal analysis of melt-crystallized nylon 6.6 is illustrated in Fig. 1a. A rather large supercooling of almost 50 K (peak to peak) characterizes cooling and heating. The glass transition is rather gradual, and the slower crystallization on quasi-isothermal cooling does not yield a major increase in crystallinity. In fact, the temperature of the melting peak

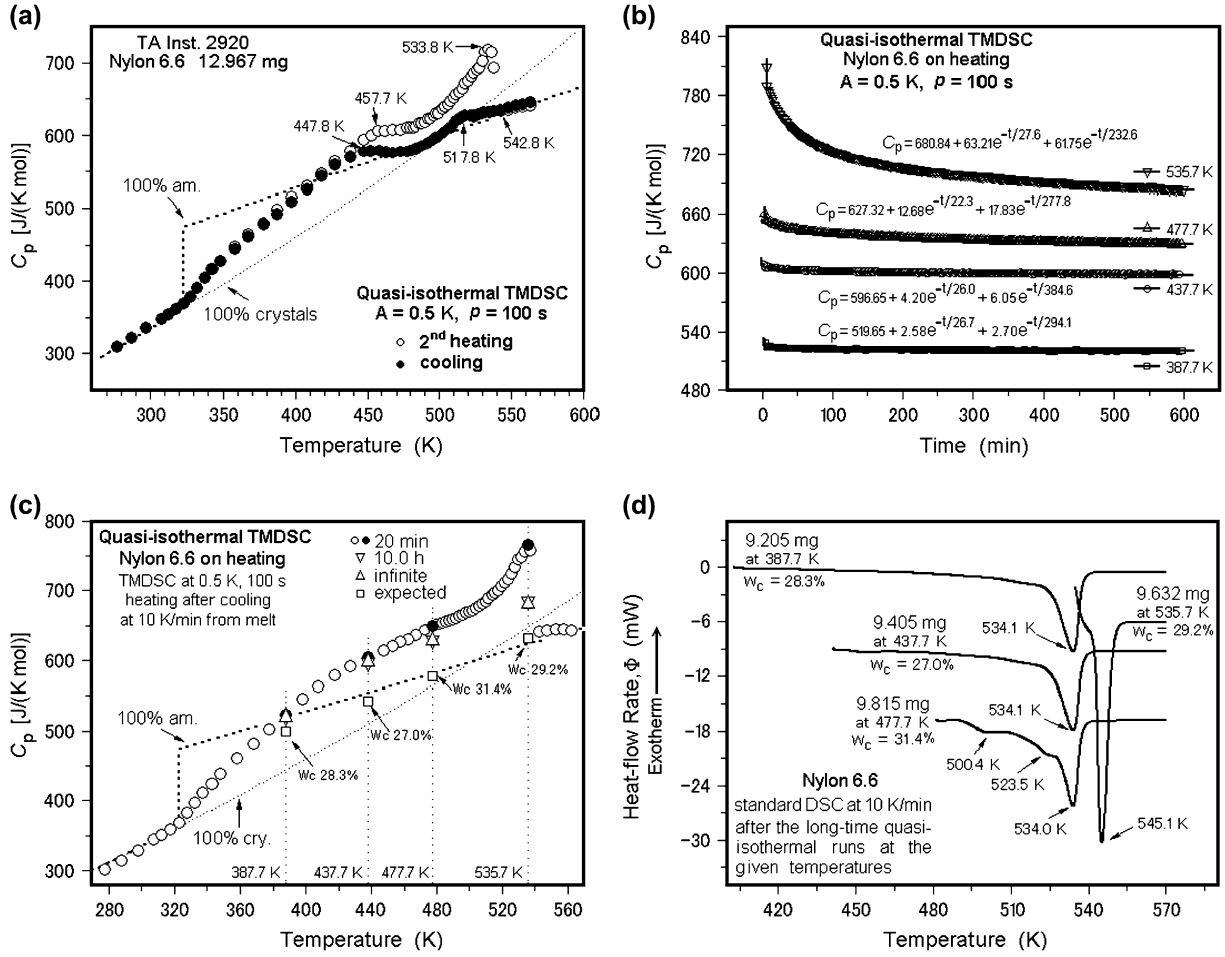

Fig. 2. Analysis of nylon 6.6 by quasi-isothermal TMDSC on cooling, followed by heating. (a) Stepwise cooling to 278 K of a 12.967 mg sample after conditioning for 10 min at 563 K, followed by stepwise heating back to 563 K (20 min quasi-isothermal runs). (b) Long-time modulation experiments. Four separate samples between 9.2 and 9.8 mg were analyzed as in (a) by cooling and followed by heating up to the given temperatures, where then a 600 min quasi-isothermal run was commenced with the shown result. (c) Comparison of data on a sample of 12.496 mg, measured as in (a), with the data in (b) and the ATHAS Data Bank heat capacities. (d) Final analyses of the samples of (b) by standard DSC immediately after completion of the long-term quasi-isothermal experiments.

decreases somewhat relative to the more quickly cooled sample, an indication that the originally poorer crystal of the center trace perfect more during heating than the slower-cooled sample of higher perfection shown in the bottom trace [23].

Fig. 1b provides a comparison of the measured C_p on heating of the sample cooled at 10 K min^{-1} (center of Fig. 1a) with the expected heat capacities calculated from the ATHAS Data Bank [10], as evaluated in Ref. [11]. The melting transition seemingly starts very gradually and develops into the major peak starting at ≈470 K with the peak positioned at 535.3 K. The glass transition begins at the expected temperature of 323 K, with its half-height at 332.7 K. On completion, at 342 K, it reaches less than 50% of the value expected for a 28% crystalline sample, which indicates a rigid-amorphous fraction, RAF, of about 36%. Beyond this temperature, the heat capacity continues to increase and reaches the level of the liquid at ≈390 K (which is close to the melting point of polyethylene, as noted earlier). This is seen not only for nylon 6.6, but also for a series of other nylons (6, 11, 12, 6.9, 6.10, and 6.12 [11]). This increase in C_p beyond 342 K may arise from the T_g of a RAF, an increase of C_p of the crystal, or possibly even from overlapping additional latent heats. The early speculative solution was that the glass transition of the RAF overlaps an increase in C_p of the crystal [11]. This issue of the thermodynamic heat capacity between T_g and T_m is taken up in this paper and advanced, based on the TMDSC results.

3.2. Temperature-modulated differential scanning calorimetry

The quasi-isothermal TMDSC runs, marked by Δ in Fig. 1c, give additional information about C_p and are compared to the center curve of Fig. 1b (solid line). An enlarged graph of the TMDSC result is shown in Fig. 1d by the points ○. The two heating modes in Fig. 1c yield identical C_ps up to ≈480 K, excluding irreversible latent heat effects due to crystal perfection as a cause of the increase in C_p. The pre-melting shoulder at 515.6 K in standard DSC is clearly non-reversible, and there seems to be a small amount of reversing melting with a peak at 535.7 K. Beyond the melting transition, the C_p of the melt is reached in the TMDSC experiments at

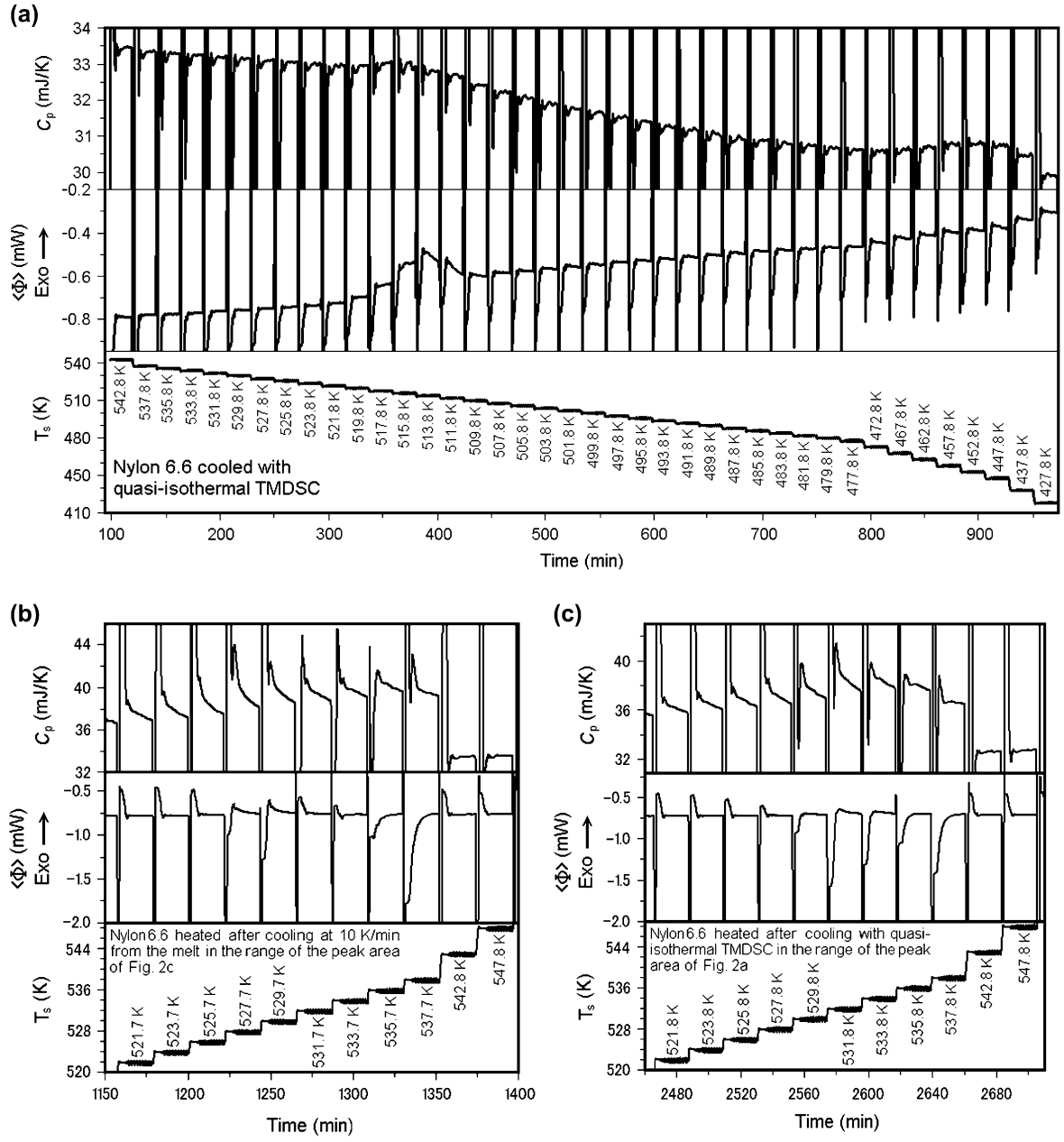

Fig. 3. Reversing sample heat capacity, C_p, heat-flow rate, $\langle\Phi\rangle$, and modulated sample temperature, T_s. (a) TMDSC on cooling as in Fig. 2a (sample of 12.967 mg). (b) TMDSC after cooling the sample at 10 K min^{-1}, covering the melting peak area of Fig. 2c (sample of 12.496 mg). (c) TMDSC after cooling in the quasi-isothermal experiment of Fig. 2a and shown in (a).

542.8 K, while the last reversing melting is seen at 537.8 K. Fig. 3c, below, shows that the heating from 537.8 to 542.8 K involves practically no further melting. This supports the suggestion that the temperature of the end of melting is set by the annealing history. On fast cooling followed by heating (Fig. 1a, center trace), the end of the melting peak occurs at ≈545 K, while after TMDSC on cooling followed by fast heating, it occurs at ≈538 K, i.e., the initially poorer crystals remain less-well annealed to higher temperature, and there, they are expected to anneal to even better crystals than the original better crystals. Note that the high-temperature leg of the DSC melting peak has an instrument lag of 1–2 K, and that long-time annealing can produce melting peaks which recover the baseline above 550 K, as can be seen in Fig. 2d, discussed below. Still, all these effects cause a recovery of the baseline which is still far below the equilibrium melting temperature, $T_m^o = 574$ K.

The quasi-isothermal TMDSC on cooling is displayed in Fig. 2a by the points ●. After this TMDSC cooling, the sample was heated by quasi-isothermal TMDSC, also displayed in Fig. 2a by the points ○. The first noticeable changes from the C_p of the melt on cooling occur at 517.8 K, only little above the temperature of first deviation of the heat-flow rate on cooling at 10 K min^{-1} in the standard DSC (Fig. 1a, top curve).

The reversing C_p on cooling matches the TMDSC on heating below 447.8 K, the temperature of the completion of crystallization by standard DSC (in Fig. 1a). Further work is needed to assess the type of crystals growing and their perfection between 517.8 and 447.8 K.

3.3. Temperature-modulated differential scanning calorimetry as a function of time

The changes of the reversing C_p with time on heating after cooling at 10 K min^{-1} is analyzed in Fig. 2b with four separate experiments of long-time annealing, extending to 600 min, chosen at strategic temperatures. The changes are compared in Fig. 2c to the 20-min modulation of Fig. 1d. It can be seen from the open and filled circles that the 20 min modulation experiments are very reproducible, and below 477.7 K only small changes occur on longer modulation, supporting the interpretation of Fig. 1c, given above.

The activation energies in Fig. 2b for the double-exponential representations change neither systematically nor to a large degree. A systematic increase with temperature, however, occurs in the pre-exponential factors. This leads to a larger reversible C_p at time infinity than expected [$C_p(\infty)$ is marked as Δ in Fig. 2c, the expected C_p as $\square$]. At 437.7 K the difference between the two C_ps reaches a maximum value of $\approx$60 J K^{-1} mol^{-1}. At the reversing melting peak, this difference in C_p has decreased only slightly to $\approx$50 J K^{-1} mol^{-1}. Fig. 2d, finally, proves that at the ends of all four long-term modulations, the crystallinity has changed only little. The multiple melting peaks in Fig. 2d mirror the degree of reorganization. Of particular interest is the sharp melting of the 29.2% crystallinity at 545.1 K after modulation at 535.7 K, which is shown in Fig. 3b to be due to melting followed by recrystallization. Note, that these crystals grew above the melting peak temperature seen by the standard DSC in Fig. 1a.

The long-time reversing modulated Φ at the four temperatures of Fig. 2b–d allows also to identify the irreversible excess in C_p as an exotherm or endotherm. Comparing the maxima and minima in Φ at short and long times shows little change at 387.7 K. A small excess in the exotherms and a decrease in the endotherms are noticeable at 437.7 and 477.7 K, indicating that the crystals which perfect during one cycle do not melt in the next. At 535.7 K, finally, both endotherms *and* exotherms are larger during the first 40 min, indicating the dynamics of melting and recrystallization. Similarly, the much larger initial irreversible melting is seen in the first few cycles, but is better seen in the recording of $\langle\Phi\rangle$ in Fig. 3, discussed next.

Fig. 3 illustrates the details in the main transition peaks by a recording of the reversing C_p of the sample as the top curves. The modulation of the sample temperature is drawn as the bottom curves. The center curves, finally, are plots of the total heat-flow rates of the sample, $\langle\Phi\rangle$, which represent the sliding average of the measured heat-flow rate over one modulation period. In case of a (metastable) steady state, the reversing C_p of the top curves should register the reversible, apparent heat capacity, which in the transition regions may contain reversible latent heat effects:

$$dH = \left(\frac{\partial H}{\partial T}\right)_{p,n} dT + \left(\frac{\partial H}{\partial n}\right)_{p,T} dn, \tag{3}$$

where dn indicates the change in composition. For crystallization and melting n can be replaced by the crystallinity, w_c, as given in Eq. (2). Since with scanning calorimetry the change in n cannot be fully controlled, one usually measures an apparent heat capacity ($= dH/dT$) and the latent heat contribution must be computed by subtracting the appropriate C_p ($= \partial H/\partial T)_{p,n}$. In steady state, the recording of $\langle\Phi\rangle$ should also reach a constant level, its deviation from zero being determined by the instrument asymmetry at the given temperature. Immediately after setting the lower or higher modulation temperature, T_o, $\langle\Phi\rangle$ registers a sharp exotherm or endotherm due to the respective heat flow needed to cool or heat the sample. This is followed by a recovery of the stationarity which may produce a small peak in the opposite direction. A short time thereafter $\langle\Phi\rangle$ should be constant, unless a slow, irreversible process is superimposed.

The TMDSC on cooling, as summarized by the data points ● in Fig. 2a, is analyzed in Fig. 3a. The TMDSC on heating of the two differently crystallized samples, summarized in Fig. 2c and a by the data points ○, is illustrated in Fig. 3b and c, respectively.

Fig. 3a shows data on cooling from the melt. A constant $\langle\Phi\rangle$ is reached down to $\approx$525 K within the 20 min of modulation and yields the expected C_p of the melt (compare to Fig. 2a). This is followed with an increasing $\langle\Phi\rangle$ with time, reaching a peak at 514 K. The exothermic $\langle\Phi\rangle$ is due mainly to the irreversible latent heat of crystallization. This crystallization continues to $\approx$510 K, beyond which a close to constant $\langle\Phi\rangle$ and C_p with time and a linear change in $(\partial C_p/\partial T)$ is observed. According to Fig. 2a, this decrease causes the heat capacity to reach again the level of the liquid. At about 480 K, C_p reverses its trend and develops a minor maximum and then follows from 447.8 K the observed C_p on heating (see Fig. 2a). The corresponding $\langle\Phi\rangle$ involves an exotherm decreasing with time which does not reach constancy after 20 min.

The reversing C_ps in Fig. 3b and c show a decrease with time of the irreversible component of the heat capacities in the melting range which is not completed at the end of the shown time-interval of 20 min. Both samples are melted at 542.8 K where C_p becomes constant after about 5 min. The initial, sharply endothermic $\langle\Phi\rangle$ and the following exothermic approach to stationarity are caused by the quick heating to the new T_o and can be assessed by comparison to the last two experiments in the melt which should show only true heat-capacity effects. The sample cooled at 10 K min^{-1} (Fig. 3b) has a somewhat higher exotherm in the first three experiments than in the reference melt, indicating an annealing of the sample even during the brief initial heating period. Starting at 527.7 K an increasingly larger endotherm due to slower partial melting is superimposed in both samples (Fig. 3b and c).

Closer inspection reveals that the melting is always coupled with some exotherm (recrystallization). The faster-cooled sample (Fig. 3b) shows clearly more exothermic annealing and recrystallization than the slower-cooled sample (Fig. 3c). Coupled with the interpretation of the multiple melting peaks, these observations are a measure of the complication of continued melting, regrowth, and perfection in nylon.

4. Final discussion

4.1. Heat capacity

The heat capacity below the reported glass transition of the amorphous nylon 6.6 at 323 K is described by the vibrational motion in the solid state [9], as is seen best in Fig. 1c. Similarly, the heat capacity above the melting is well represented by the general equation for liquid nylons:

$$C_p^{nylon} = N_C(7.4506 + 0.0745T) + N_N(86.8483 - 0.0226T) \quad (4)$$

where N_C represents the number of methylene groups (CH_2–) in the repeating unit, and N_N the number of imide groups (CO–NH–) [11].

In homologous series of polymers, the heat capacity contributions to liquid chain segments with more H-atoms increase more with temperature because of the continuing excitation of the high-frequency C–H-, N–H-, and O–H-stretching vibrations. Since the normal modes of the stretching vibrations of the heavy atoms and the bending frequencies of heavy and light atoms are usually already excited at the higher temperatures, they each contribute a constant amount to C_p ($= R = 8.3143$ J K mol^{-1}). A decreasing C_p in the liquid state is possible in the absence of many H-atoms, because the torsional vibrations of the chain atoms change to hindered rotors, which decrease their contribution to C_p, ultimately reaching $R/2$ [23]. This general behavior easily explains the opposite signs in the two parts of Eq. (4).

The C_p of the crystalline nylon 6.6 when approaching the Brill transition temperature, however, exceeds the C_p of the liquid, i.e., it must contain additional, reversible entropy contributions due to increasing disorder which occurs without a sharp phase transition and before reaching the pseudo-hexagonal crystal structure. (Note that the sample of Fig. 2c has only 28% crystallinity, making the excess heat capacity of the crystal three times as large as shown in the figure.) Beyond the Brill transition, one would expect that this high level of entropy-caused C_p of the crystal should decrease to the level of the melt since no additional disorder is attained by the pseudo-hexagonal crystal. This discussion is to be continued in Section 4.3.

4.2. Glass transition

The glass transition temperature, T_g, shifts, when taken at the mid-point of the increase of C_p, from the 323 K of amorphous nylon 6.6 to 332.7 K due to broadening of the transition, as is common in semicrystalline polymers [23]. In addition, there is evidence of 36% RAF since at 342 K the heat capacity reaches less than 50% of the value expected for a sample of 28% crystallinity (see Fig. 1c and d). The quasi-isothermal TMDSC shows no evidence of irreversible melting up to about 440 K, but a continuous increase in reversible C_p to, first, the level of the liquid (at ≈390 K), and then to an even higher level with an excess C_p of about 60 J K^{-1} mol^{-1} at ≈440 K. This makes it likely that the RAF begins its glass transition immediately above 342 K. Before this glass transition is completed, at perhaps ≈380 K, the crystal itself becomes mobile with an upper-end temperature of its glass transition at ≈440 K, which is also the approximate position of the Brill temperature, originally suggested to be at 435 K [15].

A *glass transition within the crystal* [32], as mentioned in Section 1, would parallel the increase in segmental mobility of the methylene groups. The NMR studies prove such segmental motion in the CH_2 sequences [17–20]. Quasi-elastic neutron scattering studies showed, similarly, that at temperatures 40 K below melting, the CH_2 groups undergo already large-amplitude, liquid-like motion [21]. For nylon 6.6, the same is suggested by the gradual change in the crystal from triclinic to hexagonal structure [8,22] which in its small unit cell is not commensurate with the symmetry of the CH_2 groups unless the CH_2 groups average their position due to rotational motion [4]. Finally, the expansivity of the crystals as gained from time-resolved X-ray diffraction can be analyzed as is shown in Fig. 4, based on data by Starkweather and Jones [16]. The glass transition, taken at the temperature of the change in expansivity of the crystal, occurs at about 409 K. This temperature is also in agreement with the increase in excess heat capacity starting just after the glass transition of the RAF at ≈370 K. For the sample analyzed in Fig. 2c, one, thus, can estimate the glass transition of the mobile-amorphous fraction to be at 333 K, that of the RAF at 370 K, and that of the crystal at 409 K. This is followed by the Brill transition and, finally, the melting peak at 546 K (see Fig. 2d). All these changes still occur far below the equilibrium melting temperature, estimated to be at 574 K [12–14].

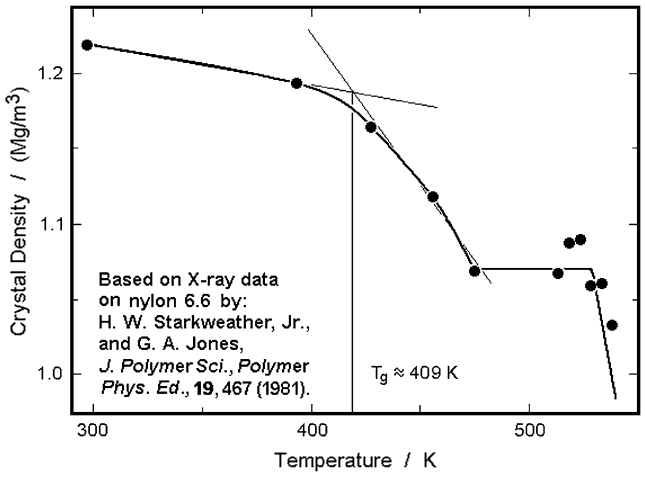

Fig. 4. Density of nylon 6.6 as a function of temperature by X-ray diffraction, illustrating a possible glass transition at the point of the changing expansivity at 409 K [6].

4.3. Melting

The irreversible melting starts at about 480 K, as discerned from Fig. 1c, and its slow completion is obvious from Fig. 2b and c. The details of melting, recrystallization, and possible annealing are seen in Figs. 2d, 3b and c. At the higher temperatures, an extensive melting followed by recrystallization is observed. This major recrystallization leads to the 4–11 K higher melting temperature observed in Fig. 2d, but even the observed lower melting temperatures are most likely increased considerably above their zero-entropy production value by crystal perfection during heating in the DSC experiment. (The zero-entropy production melting occurs at a temperature where the metastability of the initial crystal is equal to that of the supercooled melt [23].) A continuous increase in the melting peak of 70 K was proven in the past for nylon 6, which is an isomer of nylon 6.6 [33]. The crystal morphology of the nylon 6 was fixed at the various stages of perfection by arresting the reorganization with chemical cross-linking. Quite similar values are expected for the nylon 6.6.

At the temperature of the reversing, apparent C_p of nylon 6.6 in Fig. 2c, at 535.7 K, more than half of the excess reversing contribution to C_p is from slow, irreversible latent heats, which have decayed after 600 min. This leads to the final question addressed: is there any remaining reversible melting after the decay of the irreversible processes? Certainly, if one assumes the $C_p(\infty)$ (points Δ in Fig. 2c) is due to a constant excess heat capacity, there would be no significant reversible melting. The analysis of the TMDSC on cooling with Figs. 2a and 3a, however, suggests that by 510 K the increase in crystallinity is largely completed. From X-ray diffraction data taken after cooling from the melt, it was shown that the initially growing crystals are pseudo-hexagonal [22]. Fig. 3a illustrates that after the exothermic crystallization is completed at 510 K, the measured reversible C_p settles again close to the level of the liquid C_p, rather than the level measured on heating, shown in Fig. 2a. At about 440 K, in the vicinity of the Brill temperature, as the triclinic crystal structure is re-established, the heat capacity increases to that measured on heating, and then remains at lower temperatures identical to the data measured on heating. This interpretation leaves room for assignment of the difference between reversible heat capacity measured on heating and cooling to the frequently seen reversible melting [34].

4.4. Connection to other polymers

Nylon 6, as an isomer of nylon 6.6, has a polar structure along the molecules and shows two major polymorphs on crystallization from the melt which lead to multiple melting peaks with the monoclinic α-phase with anti-parallel chains in the H-bonded planes being the highest-melting crystals [5,7,8,35]. The nylon 6 does not show a distinct Brill transition to a high-temperature pseudo-hexagonal crystal phase, mainly because of its 40 K lower melting temperature than nylon 6.6 when crystallized from the melt (≈494 K), but a diffuse transition was observed close to its melting point [36]. The standard DSC curve on heating after cooling from the melt (both at 10 K min^{-1}) between the glass transition (≈322 K) and melting peak (≈492 K) of nylon 6 also is similar to nylon 6.6 within its increase in C_p beyond the calculated semicrystalline C_p (≈333 K) and liquid C_p (≈367 K) into major melting, beginning at ≈475 K [11]. These observations are indicative of similar interpretations for nylon 6 as are given here for nylon 6.6. The large-amplitude motion was also proven by quasi-elastic neutron scattering [21], and, since other nylons show this large-amplitude motion as well [8], one must assume that all aliphatic nylons with sufficiently long CH_2 sequences lose the solid nature through a glass transition below the melting point, best measured by the change of C_p [32]. Quasi-isothermal TMDSC [37] and standard DSC [11,38] are also available for nylon 12, again with quite similar increases in the excess heat capacity before irreversible melting with a peak temperature of about 452 K.

Other polymer crystals with a glass transition below the melting temperature are the aliphatic polyethers, with detailed heat capacity data by TMDSC available for poly(oxyethylene) [26] and poly(oxytetramethylene) [37,39]. Most likely polyesters, polyurethanes, and polymers with other functional groups and sufficiently long CH_2 sequences and higher melting temperatures show also separate glass transitions below the melting transitions. Similarly, all mesophases, described as liquid crystals, plastic crystals, and condis crystals, have their isotropization transition (order/disorder transitions) above the devitrification from the solid state to the mesophase [27,28]. Mesophase glass transitions have been observed for small and large molecules, attesting for the universality of the need of a glass transition when changing from the solid to a more mobile state. The novel aspect for the aliphatic nylons and polyethers is the possibility to have large-amplitude motion before changing the crystal structure from the densest packing to a mesophase of higher symmetry and larger volume. Even in polyethylene crystals, one could detect the start of large-amplitude motion in the form of *trans–gauche* flips by calorimetry, starting at ≈300 K [24,25,40], and reaching the heat capacity of the liquid at about 315 K [41].

Finally, a number of TMDSC experiments were also performed on nylon 6. Using the frequency dependence of the heat-flow rates, the irreversible, exothermic contribution could be subtracted in the melting range, and the remaining reversible melting was described by a Cole–Cole plot with a single relaxation time of ≈7 s [42] (for a discussion of these results see Ref. [34]). The rigid-amorphous fraction was recently studied by TMDSC and X-ray diffraction for nylon 6 samples of different thermal history [43]. Naturally, it would be of great interest to separate the possible glass transition of the crystal from that of the RAF and check the detailed reversing and reversible behavior of nylon 6 and several other nylons of larger and shorter CH_2 sequence length.

5. Conclusions

The irreversible, reversing, and reversible thermodynamics of semicrystalline nylon 6.6 were studied with TMDSC and

interpreted, using in addition heat capacity data from calorimetry and DSC, X-ray structure information, molecular mechanics simulations of the motion of CH_2 groups in crystals, and the results of solid-state NMR and quasi-elastic neutron scattering. This study has led to a more detailed picture of the changes which occur when heating semicrystalline nylon from the solid to the liquid state. Below the glass transition of the mobile-amorphous fraction ($T_g = 323$ K), the molecular motion consists of vibrational motion, well represented by skeletal and group vibrations [9]. As the low-temperature T_g is approached, large-amplitude motion is gradually excited, as torsional oscillations change to internal rotations. For the semicrystalline polymer, T_g is shifted to 332 K due to the presence of the crystals, and reduced in magnitude due to the presence of a rigid-amorphous fraction, RAF [11]. The, also broad, glass transition of the RAF centers at $\approx$370 K. Overlapping with the broad glass transition of the RAF is the beginning of the large-amplitude motion within the triclinic crystals, which above 390 K lead to a heat capacity larger than that of the melt because of entropy contributions within the disordering crystal. A glass transition temperature of the crystal is suggested at 409 K. At the Brill temperature, the gradual crystal disordering with a measurable entropy reaches a stable, pseudo-hexagonal, conformationally disordered state (condis crystal). Melting peaks for the differently produced samples ranged from 530 to 545 K, still much lower than the expected equilibrium melting temperature of 574 K. The crystallization on cooling at 10 K min^{-1} led to an exothermic peak at 487 K (i.e., at a supercooling of $\approx$90 K). Irreversible melting, recrystallization, and crystal perfection were observed from 480 K on and its kinetics was extrapolated to infinite time where fast reversible processes remain. There may be some reversible melting on the crystal growth faces over a wide temperature range up to the upper limit of irreversible melting. This research suggests that all other aliphatic nylons, as well as other macromolecules of sufficiently long CH_2 sequences, may show a similar glass transition within the crystal coupled with increasing disorder, which may or may not lead to a mesophase. The transition from the crystal to the mesophase may be gradual (as seen in nylon 6.6), occur at a sharp, first order transition, or be a combination of both as seen earlier [27,28].

Acknowledgments

This work was supported by the Division of Materials Research, National Science Foundation, Polymers Program, Grant # DMR-0312233, and by the Division of Materials Sciences and Engineering, Office of Basic Energy Sciences, U.S. Department of Energy at Oak Ridge National Laboratory, managed and operated by UT–Battelle, LLC, for the U.S. Department of Energy, under contract number DOE-AC05-00OR22725.

References

[1] Mark H, Whitby GE. Collected papers of Wallace H. Carothers on polymerization. New York: Interscience; 1940.
[2] Kohan MI, editor. Nylon plastics handbook. Cincinnati: Hanser Gardener; 1995.
[3] Flory PJ. Statistical mechanics of chain molecules. Wiley-Interscience; 1969.
[4] Kitaigorodskii AI. Organicheskaya Kristallokhimiya. Moscow: Press of the Academic Science USSR; 1955 (Revised, English translation by Consultants Bureau: New York, 1961).
[5] Wunderlich B. Macromolecular physics. In: Crystal structure, morphology, defects, vol. 1. Academic Press; 1973.
[6] Bunn CW, Garner EV. Proc R Soc London 1947;A189:39.
[7] For a collection of a larger number of nylon crystal structures, see: Miller RL. Crystallographic data and melting points for various polymers. In: Brandrup J, Immergut EH, Grulke EA, Abe A, Bloch DR, editors. Polymer handbook. Part VI: Solid state properties. 4th ed. Wiley, ISBN 1-59124-883-3; 1999. Revised Ed., Electronic Ed. 2005.
[8] For a detailed discussion of crystal structures and morphologies of nylons see also Xenopolous A, Clark ES, in Section 5 of Ref. [2].
[9] Xenopoulos A, Wunderlich B. Polymer 1990;31:1260.
[10] Gaur U, Lau S-F, Wunderlich BB, Wunderlich B. J Phys Chem Ref Data 1983;12:65, extended by new measurements in Refs. [9,11]; See also: Wunderlich B. The Athas Data Base on heat capacities of polymers. Pure Appl Chem 1995;67:1019. For a collection of the updated critically analyzed data, see: our website at the address: http://athas.prz.rzeszow.pl.
[11] Xenopoulos A, Wunderlich B. J Polym Sci Polym Phys Ed 1990;28:2271.
[12] Haberkorn H, Illers K-H, Simak P. Colloid Polym Sci 1979;257:820.
[13] Magill JH, Girolamo M, Keller A. Polymer 1981;22:43.
[14] Xenopoulos A. Thermal analysis and studies of conformational disorder in aliphatic polyamides. Thesis, Rensselaer Polytechnic Institute, Chemistry: Troy, NY; 1990.
[15] Brill R. J Prakt Chem 1942;161:49.
[16] Starkweather Jr HW, Jones GA. J Polym Sci Polym Phys Ed 1981;19:467.
[17] Slichter WP. J Polym Sci 1958;35:77.
[18] Hirschinger J, Miura H, Gardner KH, English AD. Macromolecules 1990;23:2153.
[19] Miura H, Hirschinger J, English AD. Macromolecules 1990;23:2169.
[20] Wendoloski J, Gardner KH, Hirschinger J, Miura H, English AD. Science 1990;247:431.
[21] Xenopoulos A, Wunderlich B, Narten AH. Macromolecules 1993;26:1576.
[22] Xenopoulos A, Wunderlich B. Colloid Polym Sci 1991;269:375.
[23] Wunderlich B. Thermal analysis of polymeric materials. Berlin: Springer; 2005.
[24] Wunderlich B, Sullivan P, Arakawa T, DiCyan AB, Flood JF. J Polym Sci Part A Polym Chem 1963;1:3581.
[25] Sumpter BG, Noid DW, Liang GL, Wunderlich B. Atomistic dynamics of macromolecular crystals. In: Suter U, Monnerie L, editors. Atomistic modeling of physical properties of polymers. Berlin: Springer; 1994 [Adv Polym Sci 116].
[26] Qiu WL, Pyda M, Nowak-Pyda E, Habenschuss A, Wunderlich B. J Polym Sci Part B Polym Phys, in press.
[27] Wunderlich B, Grebowicz J. Adv Polym Sci 1984;60/61:1.
[28] Wunderlich B, Möller M, Grebowicz J, Baur H. Conformational motion and disorder in low and high molecular mass crystals. Berlin: Springer; 1988 [Adv Polym Sci 87].
[29] Gmelin SME, Höhne GWH, Cammenga HK, Hemminger W, Eysel W. Thermochim Acta 1994;247:129.
[30] Ishikiriyama K, Wunderlich B. J Therm Anal 1997;50:337.
[31] Kwon YK, Androsch R, Pyda M, Wunderlich B. Thermochim Acta 2001;367/368:203.
[32] Wunderlich B. Thermochim Acta 2006;446:128.
[33] Todoki M, Kawaguchi T. J Polym Sci Polym Phys Ed 1977;15:1067, 1507.
[34] Wunderlich B. Prog Polym Sci 2003;28/3:383.
[35] Wunderlich B. Macromolecular physics. In: Crystal melting, vol. 3. Academic Press; 1980. p. 186–9.

[36] Murthy NS, Curran SA, Aharoni SM, Minor H. Macromolecules 1991; 24:3215.
[37] Di Lorenzo ML, Pyda M, Wunderlich B. J Polym Sci Part B Polym Phys 2001;39:2969.
[38] Di Lorenzo ML, Pyda M, Wunderlich B. J Polym Sci Part B Polym Phys 2001;39:1594.
[39] Pak J, Pyda M, Wunderlich B. Thermochim Acta 2003;396: 43.
[40] Wunderlich B, Baur H. Fortschr Hochpolymeren Forsch [Adv Polym Sci] 1970;7:151.
[41] Pak J, Wunderlich B. Macromolecules 2001;34:4492.
[42] Toda A, Tomita C, Hikosaka M. J Therm Anal 1998;54:623.
[43] Chen H, Cebe P. Investigation of the rigid amorphous fraction in nylon-6. In: Vitaz I, Rich MJ, Schoch KE, editors. Proceedings of 34th NATAS conference in Bowling Green, KY, August 6–9, vol. 34; 2006. CD ed, 008-11-088/1-07.